

## SEISMIC PERFORMANCE OF COLUMNS AND BEAM-COLUMN JOINTS IN COMPOSITE CES STRUCTURAL SYSTEM

Toshiaki Fujimoto<sup>1</sup>, Hiroshi Kuramoto<sup>2</sup> and Tomoya Matsui<sup>3</sup>

<sup>1</sup> Senior Research Eng., Ando Corp. Research Center, Saitama, Japan

<sup>2</sup> Professor, Dept. of Architectural Engineering, Osaka University, Suita, Japan

<sup>3</sup> Assistant Prof., Dept. of Architecture & Civil Eng., Toyohashi University of Technology, Aichi, Japan

Email: fujimoto-toshiaki@ando-corp.co.jp, matsui@tutrp.tut.ac.jp and kuramoto@arch.eng.osaka-u.ac.jp

### ABSTRACT:

Concrete Encased Steel (CES) structural system consisting of fiber reinforced concrete (FRC) and encased steels only is a new composite structural system proposed by the authors, and is being conducted continuous and comprehensive studies to make it practical. Experimental studies on CES structural system have been carried out in the past about ten years. To date, seismic behavior of CES columns was investigated to reveal the synergistic interaction between FRC and encased steels, and to evaluate the stiffness, flexural strength and hysteresis characteristics, in which the main test parameters were the section shape of encased steels, the type and content of fibers used for FRC and the applied axial load levels. CES beam-column joints were also tested to investigate the seismic behavior of both interior and exterior joints. This paper summarizes the test results and discusses how to evaluate the structural characteristics to be required in the structural design practice such as the cracking, yield and ultimate strengths and the hysteresis characteristics of CES columns and beam-column joints. The test results show that the CES columns and beam-column joints have excellent seismic performance with a stable spindle-shape hysteresis characteristic, which are better than those of SRC columns and beam-column joints. It is revealed based on the test results that the AIJ design formulas for SRC structures can be applied for evaluating the ultimate strengths of CES columns and beam-column joints. Hysteresis models for CES columns are also proposed and verified their validity for the practical use through comparing them with the test results.

**KEYWORDS:** CES Structural System, Seismic Performance, Ultimate Strength, Hysteresis Model

### 1. INTRODUCTION

Steel reinforced concrete (SRC) structures are typical composite structural systems consisting of steel and reinforced concrete (RC), which have an excellent earthquake resistance with high capacities and deformability. However, the design process and construction work are more complicated than those for RC structures and steel structures. In order to solve these problems, Concrete Encased Steel (CES) structural system consisting of fiber reinforced concrete (FRC) and encased steels only have been proposed by the authors as a new composite structural system, and is being conducted continuous and comprehensive studies to make it practical. Experimental studies on CES structural system have been carried out in the past about ten years. To date, seismic behavior of CES columns was investigated to reveal the synergistic interaction between FRC and encased steels, and to evaluate the stiffness, flexural strength and hysteresis characteristics. CES beam-column joints were also tested to investigate the seismic behavior of both interior and exterior joints. This paper summarizes the test results and discusses how to evaluate the structural characteristics to be required in the structural design practice such as the cracking, yield and ultimate strengths and the hysteresis characteristics of CES columns and beam-column joints. Analytical models to represent the hysteretic behavior of CES columns is also presented.

### 2. OUTLINE OF TEST PROGRAM

#### 2.1 Test Program on CES Columns

To investigate the effects of the section shape of encased steels, the type and content of fibers used for FRC and the applied axial load levels on the seismic behavior of CES columns, nine specimens were tested under cyclic loading. The dimensions and details of the specimens are shown in Figure 1 and Table 1. The material strength of built-in steels and concrete are also listed in Table 1. Specimens SC, VF1, VF2 and SF2 were designed to examine the effect of the type and content of fibers used for FRC on the seismic behavior of the CES columns.

Normal concrete was used for the specimen SC, and FRC was used for specimens VF1 (poly vinyl alcohol (PVA) fiber, mixing volume=1%), VF2 (PVA fiber, 2%), SF2 (stainless steel fiber, 2%). Specimens VF2N3, VF2N5 and VF2NV were planned compared with influence of axial load level. Steel encased in these columns had a cross shape section combining two H-section steels, and CESU had single H-section steel.

Figure 2 illustrates the test setup and the loading condition of specimen. The test setup was designed to subject specimen to an axial load and horizontal displacement reversals in a double curvature condition with the point of inflection occurring at the middle height. The footing and top stub were fixed to the reaction floor and the loading beam using the tension rods, respectively. Two vertical hydraulic jacks applied an axial load, and held the top stub in parallel with the footing at the same time. A horizontal hydraulic jack applied horizontal load by controlling the displacement. A constant compressive axial load was applied on specimens SRC, SC, VF1, VF2, SF2, VF2N3, VF2N5 and CESU. A variable axial load with tension and compression was applied on specimen VF2NV. The incremental loading cycles were controlled by story drift angles,  $R$ , defined as the ratio of lateral displacements to the column height,  $\delta/h$ . The lateral load sequence consisted of two cycles to each story drift angle,  $R$  of 0.005, 0.01, 0.015, 0.02, 0.03 and 0.04 radians followed by half cycle to  $R$  of 0.05 rad.

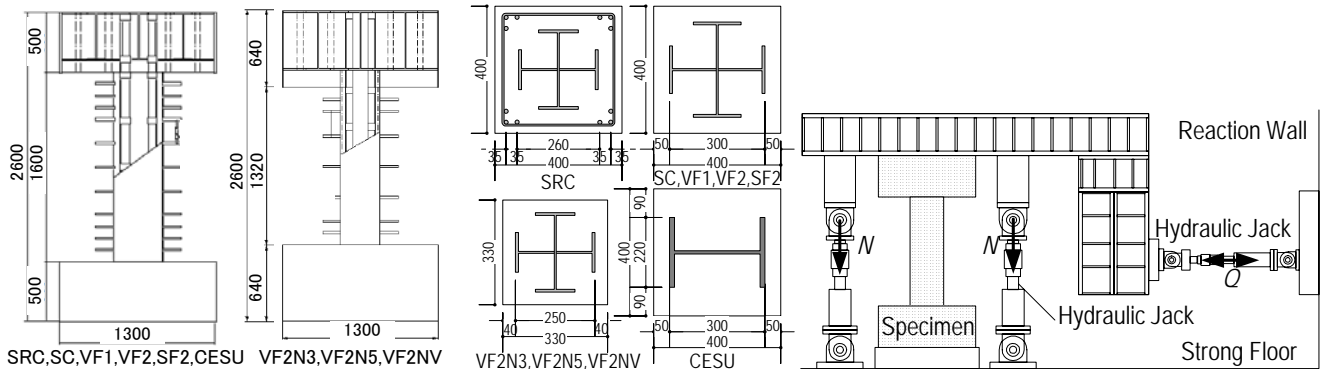


Figure 1 Test specimens

Figure 2 Schematic view of test setup

Table 1 Details of test specimen

Specimen		SRC	SC	VF1	VF2	SF2	VF2N3	VF2N5	VF2NV	CESU	
Reinforced fiber	Fiber type	-	-	PVA		Stainless	PVA				
	Mixing volume	-	-	1.00%	2.00%	2.00%	2.00%				
Cross section: $b \times D$		400 x 400				330 x 330			400 x 400		
Concrete strength: $\sigma_B$ (MPa)		35.5	37.3	52.3	55.5	65.3	46	38	33.5		
Column height: $h$ (mm)		1600				1320			1600		
Built-in steel	Shape		Double H-section						Single H-section		
	Cross section		250×125×6×9	300×150×6.5×9			250×125×6×9		300×220×10×15		
	Yield stress: $\sigma_y$ (MPa)	Flange	300	323	337		335		289		
Web		347	412	364		393		299			
Axial force	Condition		Constant					Variable		Constant	
	$N$ (kN)		1100				1500	2380	2380	-910	1600
Axial load level: $N/N_o^*$		0.15	0.14	0.11	0.11	0.09	0.22	0.40	0.40	-0.15	0.17

\*:  $N_o = \sigma_{cu} \cdot \sigma_B \cdot \alpha_A + \sigma_y \cdot \alpha_A$ ,  $N_o$ : Axial strength of CES beam-columns,  $\sigma_{cu}$ : Reduction factor of concrete ( $\sigma_{cu} = 0.85 - s_p c$ ,  $s_p = s_a c / bD$ ,  $s_a$ : Sectional area of steel flange on compressive side),  $\alpha_A$ : Sectional area of concrete,  $\alpha_A$ : Sectional area of Steel

## 2.2 Test Program of Beam-Column Joints

A total of six specimens were tested; four interior (specimens CESJ-A, CESJ-B, CESJ-C and CESJ-D) and two exterior (specimens CESJ-AE and CESJ-BE) joint specimens. The shape and the material strengths of the specimens are shown in Table 2. The dimensions and details of the specimens are shown in Figure 3. All specimens had a column with 400 mm square section and beam with 300x400 mm section. The main test parameter was the types of failure mode; beam flexural failure and joint shear failure. Specimens CESJ-A, -C, -D and -AE were designed to have a beam flexural failure and the others (CESJ-B and -BE) were designed to have a joint shear failure. The ultimate strengths of the columns and beams were calculated by the superposition method, and that of the joint panels were calculated by the shear design equation of (AIJ 2001). The steel encased in each column had a single H-section steel of 300x220x10x15 mm. For specimens designed for beam

flexural failure, the steels encased in the beam were H-300x150x6.5x9, while for Specimens designed for joint shear failure, they were H-300x200x9x19. As for specimens CESJ-B and -BE, the steel web thickness of the joint is significantly smaller than that of the column, which was intentionally designed to ensure the shear failure to take place at the joint. As for specimen CESJ-C, thicker plate was used for the flange and stiffener of panel zone differs from CESJ-A. Furthermore, thicker web plate was used for the panel web in specimen CESJ-D. FRC (PVA fiber, 1%) was used for all specimens.

The loading condition is shown in Figure 4. The interior joint specimens were loaded lateral cyclic shear forces by a horizontal hydraulic jack at the top of the column while a constant compression load was applied by two vertical hydraulic jacks. The magnitude of the applied compression load was 775kN( $N/bD\sigma_B$ : 0.15). For the exterior joint specimens, a varying axial load,  $N$  ( $=0.1N_o\pm 3Q$ , where  $Q$  = applied shear force) was applied. The reaction stringer absorbed the shear forces in the beam caused by the load applied at the top of the column. The incremental loading cycles were controlled by story drift angles,  $R$ , defined as the ratio of relatively vertical displacement at the beam end to the beam length,  $\delta/L$ . The loading scheme was the same as column tests.

Table 2 Details of test specimen

Specimen	CESJ-A	CESJ-B	CESJ-C	CESJ-D	CESJ-AE	CESJ-BE
Shape	Interior Joints				Exterior Joints	
Concrete strength: MPa	33.3	31.6	31.7	33.4	38.4	40.0
Column	Built-in steel: (mm)		H-300x220x10x15			
	Yield stress: $\sigma_y$ (MPa)	Flange	284		294	304
		Web	296		320	319
	Column height: $h$ (mm)		1300			
Cross section: $b \times D$ (mm)		400x400				
Beam	Built-in steel: (mm)		H-300x150x6.5x9	H-300x200x9x19	H-300x150x6.5x9	H-300x200x9x19
	Yield stress: $\sigma_y$ (MPa)	Flange	321	252	270	304
		Web	408	293	324	348
	Beam length: $l$ (mm)		2250			1125
Cross section: $b \times D$ (mm)		300x400				
Panel	Thickness: (mm)	Flange	15		15	
		Stiffener	9	19	16	
		Web	10	4.5	10	19
	Yield stress: $\sigma_y$ (MPa)	Flange	284		265	
		Stiffener	321	252	319	304
		Web	296	257	276	250

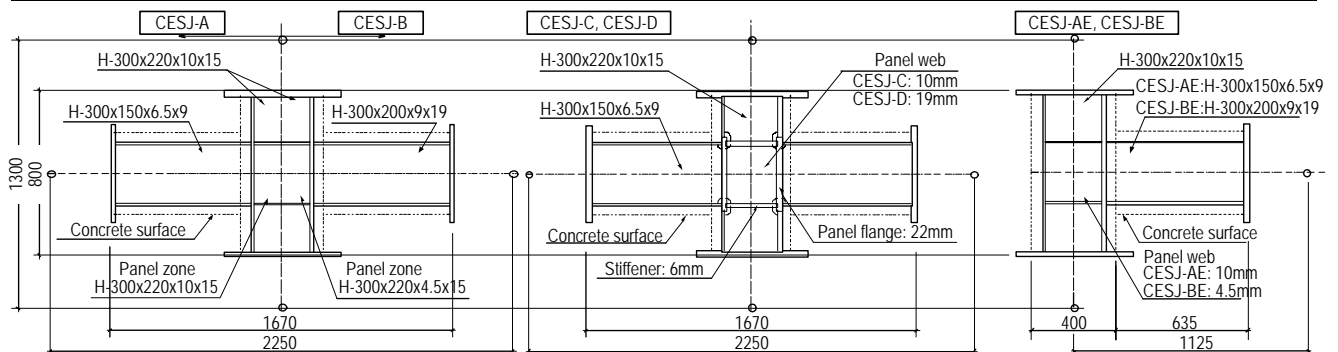


Figure 3: Details of test specimen

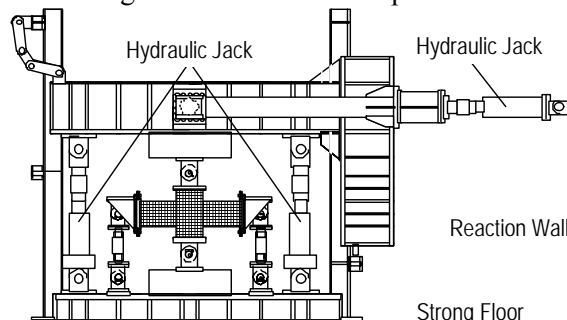


Figure 4 Schematic view of test setup

### 3. EXPERIMENTAL RESULTS AND DISCUSSIONS

#### 3.1 CES Columns

##### 3.1.1 Hysteresis characteristics and failure modes

Shear versus story drift angle relationships of all specimens are given in Figure 5. Crack modes on column faces of all specimens after loading are also presented in Photo 1. From Figure 5, it can be seen that all specimens showed very ductile and stable spindle-shaped hysteresis loops. In specimen SRC, cover concrete had crushed in flexure at both the top and bottom of the column at story drift, R of 0.015 rad., and buckling occurred at the reinforced bar at story drift, R of 0.04 rad. From the photo, it can be seen that specimen using normal concrete, SC had the most damages, in which the severe shear cracks of the cover concrete occurred. Moreover, cover concrete away from the column face with an increase of the story drift angle. In specimens VF1, VF2 and SF2, the brittle failure was not significant during testing. Although the small cracks propagated at R of 0.04 rad. The damage of the columns was less than that of specimen SC due to the enhancement of the ductility on the concrete by the fibers. From above mentioned, the type of concrete greatly affected the observed cracking patterns of the CES column. This indicates that the encased concrete used for FRC has a significant influence on the damage of CES columns. In specimen applied high axial load (VF2N3 and VF2N5), the hysteresis curve showed a stable behavior with a little strength degradation after attaining the maximum capacity at R of 0.015 rad. In the specimen applied varying axial load (VF2NV), the maximum strength was reached at R of 0.015 rad. under compressive axial load and at R of -0.04 rad. under tensile axial load, and no drastic strength reduction was observed. As revealed by comparing the hysteresis loops and damage situations of these specimens, the FRC contributed to improve the structural performance and reduce the damage in composite columns.

##### 3.1.2 Ultimate strength

The experimental maximum strengths,  $Q_{exp}$  are listed in Table 3, compared with the calculated flexural strength,  $Q_{bu}$  and shear strength,  $Q_{su}$ . The flexural strength,  $Q_{bu}$  was calculated by the superposition method, the shear strength,  $Q_{su}$  was also calculated by (AIJ 2001). The maximum strengths of all specimens except for specimen

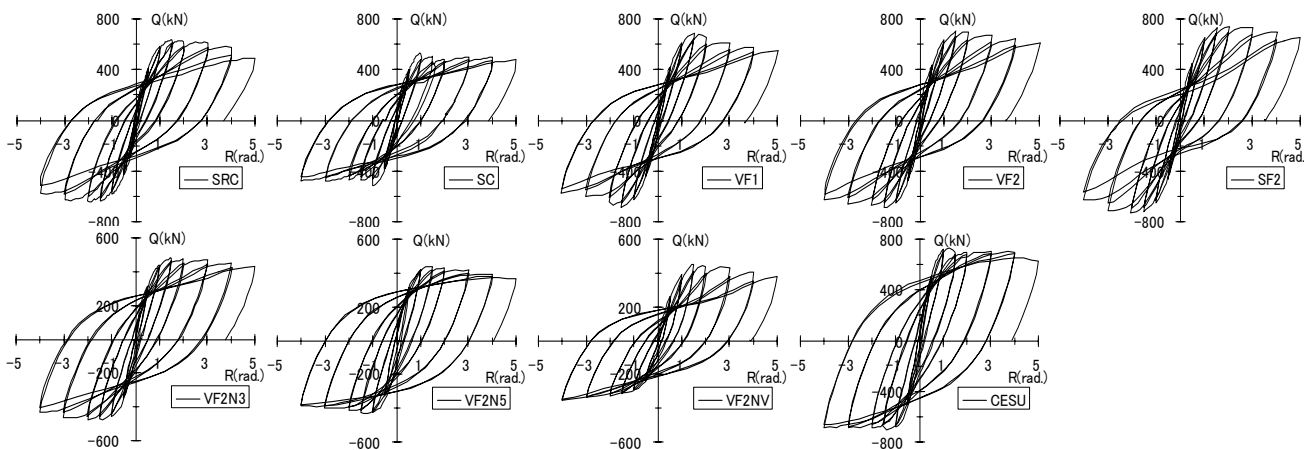


Figure 5 Shear force - story drift angle relationships

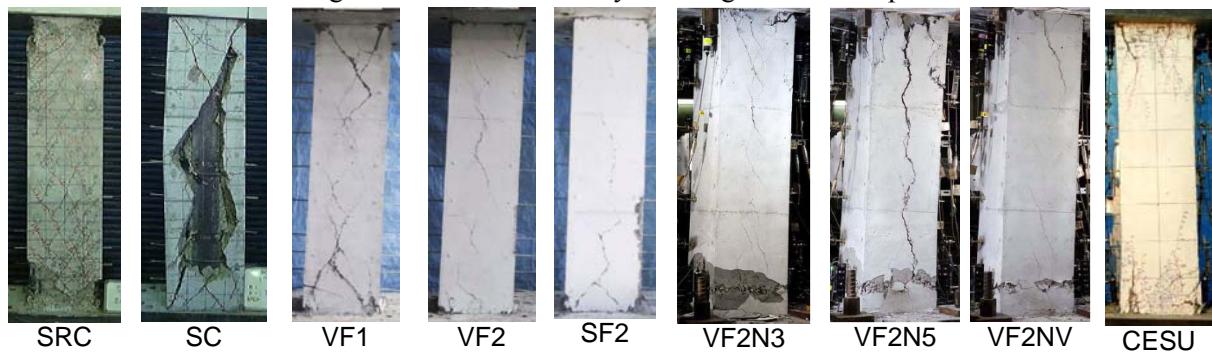


Photo 1 Crack modes of specimens after loading

SC indicated larger than the calculated flexural strength  $Q_{bu}$ . The experimental strength of CES columns using FRC is 1.0-1.14 times the calculated flexural strength. It is understood that the experimental flexural strengths fairly agreed with the calculated strengths. On the other hand, calculate shear strength,  $Q_{su}$  of these specimens displayed smaller values compared with calculated flexural strength,  $Q_{bu}$ . However, severe shear cracks of the cover concrete were not observed (see photo 1). This means that it is necessary to consider the effect of strength enhancement using FRC in estimating the shear strength of CES columns.

Table 3 Comparison between calculation strength and test results

Specimen		SRC	SC	VF1	VF2	SF2	VF2N3	VF2N5	VF2NV	CESU
Test	$Q_{exp}$ (kN)	638	527	689	703	738	481	439	454 (-353)	734
Cal.	$Q_{bu}$ (kN)	527	566	645	660	698	479	433	433 (-309)	650
	$Q_{su}$ (kN)	621	593	569	575	593	430	421	421	720
	$Q_{su}/Q_{bu}$	1.18	1.05	0.88	0.87	0.85	0.90	0.97	0.97(1.36)	1.11
	$Q_{exp}/Q_{bu}$	1.21	0.93	1.07	1.07	1.06	1.00	1.01	1.05 (1.14)	1.13

### 3.2 CES Beam-Column Joints

#### 3.2.1 Hysteresis characteristics and failure modes

Story shear versus story drift angle relationships of all specimens are given in Figure 6. In this figure, first yield point of steel beam is shown in the circle mark. Failure modes of all specimens at R of 0.03 radians are also shown in Photo 2. In specimen with beam flexural failure, the first yielding occurred on steel flange of the beam at R of 0.005 rad. Maximum shear capacity was reached at R of 0.03 rad. These specimens showed a stable spindle-shape hysteresis loop with a little strength degradation after reaching the maximum capacity. The specimens CESJ-C and CESJ-D showed a strength degradation in the loading cycle of R=4% due to the crack occurring at the beam end. In specimen with panel shear failure, the first yielding occurred on steel web of the panel zone. Subsequently, the shear cracks occurred in concrete panel, although the cracks propagated. Compared to specimens with beam flexural failure, more damages of the concrete panel were observed in these specimens, as shown in Photo 2. The hysteresis curves of these specimens showed a little pinching-shaped but stable behavior with strength degradation after attaining the maximum capacity.

#### 3.2.2 Deformation contributions of each component

Figure 7 shows the panel shear  ${}_pQ_c$  versus joint distortion responses  $\gamma_p$  for all specimens until story drift angle, R of 0.03 rad. The joint distortion,  $\gamma_p$ , on the horizontal axes was calculated using Eqn. 2. Figure 8 shows the definition to calculate the joint distortion.

$${}_pQ_c = Q_b \cdot l' \cdot \left( \frac{l - j_c}{l' \cdot j_b} - \frac{l}{l' \cdot h} \right) \quad \text{for interior joint,} \quad {}_pQ_c = \frac{Q_b \cdot l'}{2} \cdot \left( \frac{l - j_c}{l' \cdot j_b} - \frac{l}{l' \cdot h} \right) \quad \text{for exterior joint} \quad (1)$$

$$\gamma_p = \frac{\sqrt{h_p^2 + l_p^2}}{h_p \cdot l_p} \cdot \frac{\delta_1 - \delta_2}{2} \quad (2)$$

From Figure 7, it can also be seen the different joint shear distortion values of specimens. The hysteresis curves of CES joint showed a little pinching-shaped but stable behavior with strength degradation after attaining the maximum capacity. The maximum strength of the joint was reached at  $\gamma_p$  of 0.01-0.02 rad. Figure 9 shows the contributions of deformation by the column, beam and joint panel to the total deformation of the specimen until R of 0.02 rad. The values were obtained by measuring the deformations of beam, column and panel zone, as described in Figure 8. The deformations of the column and the joint panel were converted into the deformation of beam, as described in Figure 10. It is clearly seen from Figure 9 that the beam contributed the biggest deformation for specimens with beam flexural failure, while in specimen with joint shear failure the biggest deformation was contributed by the joint panel. This indicates that these contributions showed a good agreement with the expected failure mode of the joints.

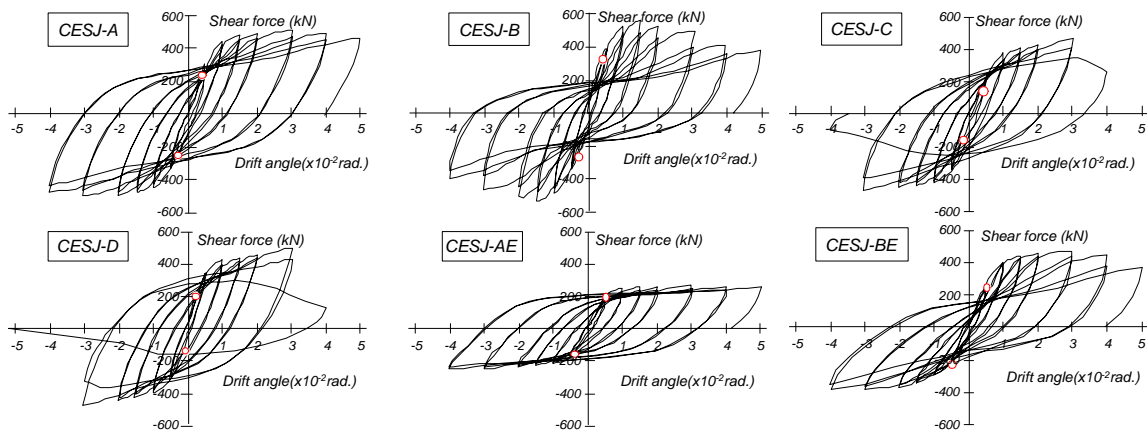


Figure 6 Story shear-story drift angle relationships.

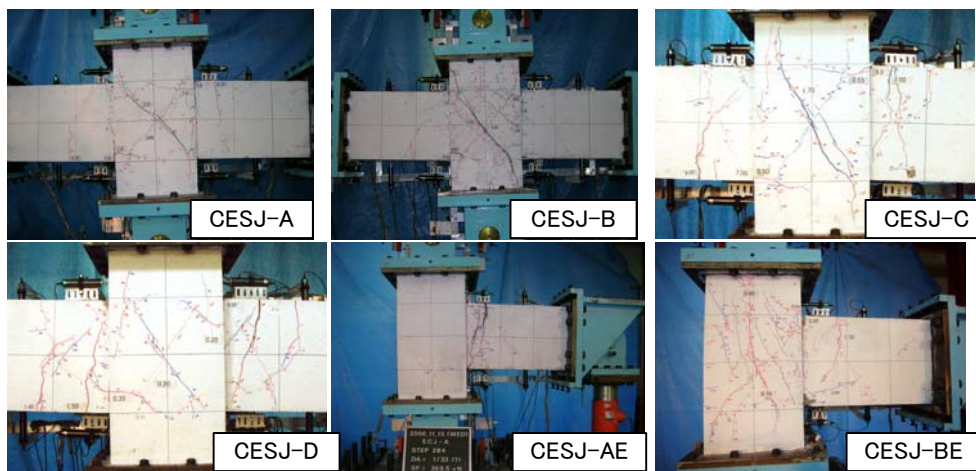


Photo 2 Crack modes of specimens at R of 0.03rad.

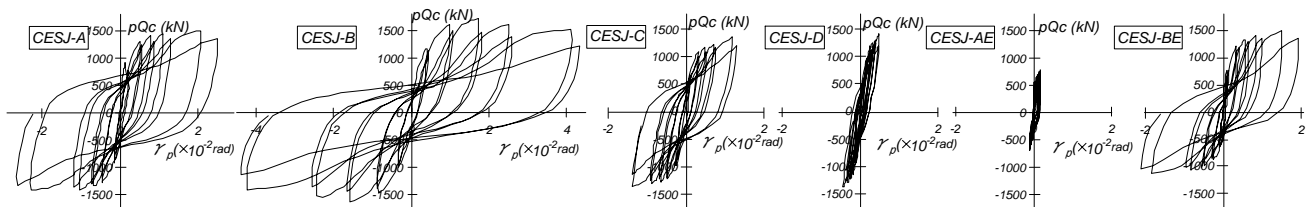


Figure 7 Panel shear  $pQ_c$  versus joint distortion responses  $\gamma_p$

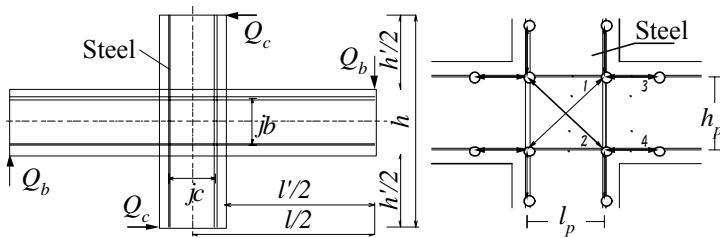


Figure 8 Definition of joint distortion and measurement

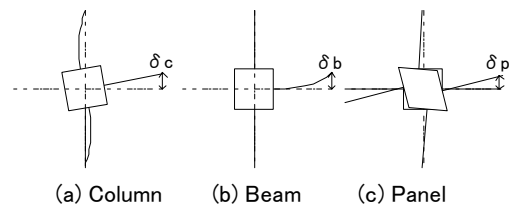


Figure 10 Definition of deformations

### 3.2.3 Ultimate strength

The superposition method was used to calculate the maximum strengths of the column and beam, respectively, while the joint panel strength,  $Q_{pcal}$  was calculated by (AIJ 2001) using Eqn. 3. To facilitate comparison between the joint panel strength,  $Q_{pcal}$  and the maximum shear load obtained from the experiment calculated from Eqn. 4 must be transferred to the design shear at the column,  $cQ_{pcal}$ .

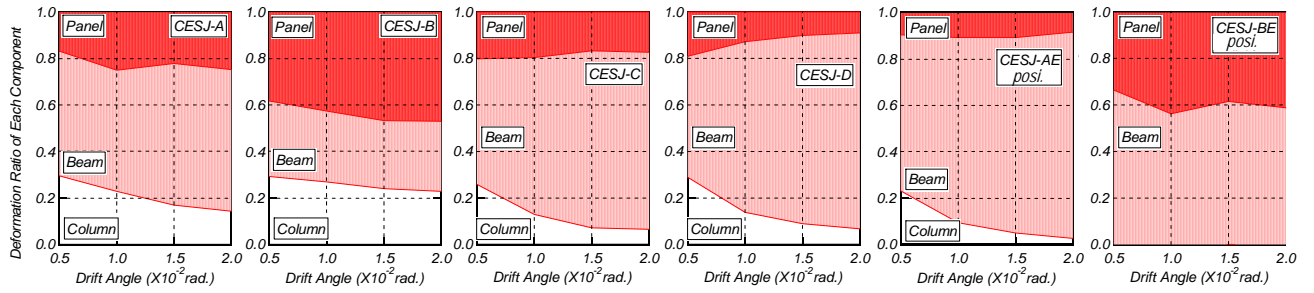


Figure 9 Deformation ratio of each component

$$Q_{pcal} = J F_s \cdot J \delta_c \cdot c A_e + 1.2 \cdot {}_{sw} \sigma_y \cdot {}_{sw} A / \sqrt{3}, \quad J F_s = \min(0.12 \sigma_B, 1.8 + 3.6 \sigma_B / 100) \quad (3)$$

$${}_c Q_{pcal} = \frac{j_b \cdot l}{(l - j_c) \cdot h - j_b \cdot l} \cdot Q_{pcal} \quad (4)$$

Where,  ${}_J F_s$ : ultimate shear strength of concrete,  ${}_J \delta_c$ : geometric factor (3 for interior joint, 2 for exterior joint),  $A_e$ : effective sectional area of concrete in the joint panel (column depth in joint panel x average of column and beam width),  ${}_{sw} \sigma_y$ : Yield stress of steel web in the joint panel,  ${}_{sw} A$ : sectional area of steel web in the joint panel.

Table 4 shows the calculated maximum strengths of the column, beam and joint panel, which were compared with the test results. The calculated strengths and the test result loads in the table are shown by the column shear force. In Specimens with beam flexural failure, the measured strength agreed with the calculated strength of the beam, while the calculated joint panel strength was higher than the measured strength. The measured strength was a value from 0.97 to 1.26 times calculated strength. This indicated that the yielding of the beam first occurred before yielding of the joint panel. For specimen with joint shear failure, the calculated strength of the joint panel was slightly less than the measured strength, and indicated 1.27 to 1.57 times the value. These comparative results indicated that the calculation method could be used to predict the ultimate strength of CES joint panels.

Table 4 Comparison between calculation strength and test results

Specimen	CESJ-A	CESJ-B	CESJ-C	CESJ-D	CESJ-AE	CESJ-BE
$Q_{cu}$ (kN)	1123	1117	1193	1209	1348 (922)	1447 (800)
$Q_{bv}$ (kN)	466	716	459	461	214	394
$Q_{pv}$ (kN)	511	364	497	643	436	302
$Q_{exp}$ (kN)	516.5	564.0	467.5	500.0	269.5 (-263.5)	473.0 (-383)
$Q_{exp} / \min(Q_{bv}, Q_{pv})$	1.11	1.55	1.02	1.08	1.26 (1.23)	1.57 (1.27)

## 4. HYSTERETIC MODEL FOR BEHAVIOR OF CES COLUMNS

### 4.1 Skeleton and Hysteretic Model

As illustrated in Fig. 11, the skeleton curve of shear-rotation angle relationship of CES columns subjected to cyclic lateral loading and a constant axial load can be expressed by the tri-linear skeleton model. This model is defined by the following four parameters: the elastic stiffness  $K_e$ ; the shear force at the first bending point  $Q_c$ ; the stiffness degrading ratio at the second bending point  $\alpha_y$ ; and the shear strength at the second bending point  $Q_y$ . The behavior of CES columns is assumed to be elastic until the first bending point.  $Q_c$  is assumed to the bending crack strength based on (AIJ 1999).  $Q_y$  is given by the calculate flexural strength prescribed in the (AIJ 2001).  $\alpha_y$  was given by the ratio of  $K_2$  to  $K_e$ , where  $K_2$  was determined that area A was equal to area B as shown in Fig. 11. As illustrated in Fig. 12, the hysteretic curve of shear-rotation angle relationship of CES columns can be expressed by the degrading tri-linear model. In this model, half cycle curve of test result is modeled by tri-linear. Stiffness  $K_r$  was reduced by the maximum rotation angle  $R_m$  as shown in Eqn. 5. Stiffness degrading point  $\beta Q_m$  was defined that energy of test result was equivalent to the model.

$$K_r = K_e \times |R_m / R_c|^{-\alpha}, \quad \alpha: \text{stiffness reduction factor} \quad (5)$$

#### 4.2 Comparisons between Proposed Model and Test Results

The effects of test parameters (section shape of encased steels, the type and content of fibers used for FRC and the applied axial load levels) on  $\alpha_y$ ,  $\alpha$  and  $\beta$  were investigated based on the test result. As a result, it was concluded that no or very weak correlations existed between the test parameters and  $\alpha_y$  or  $\alpha$ . Accordingly, the average values of the test result,  $\alpha_y=0.3$  and  $\alpha=0.4$  were proposed to be used in modeling. Difference was observed between  $\beta$  and maximum rotation angle, and following equation was proposed.

$$\beta = (53.4 N/N_u - 44)R_m + 1 \quad \text{for } R \leq 0.02 \text{ rad.}, \quad \beta = 1.07 N/N_u + 0.12 \quad \text{for } R > 0.02 \text{ rad.} \quad (6)$$

Fig. 14 shows comparisons between the proposed hysteretic model and the test results of CES specimens under the constant axial load. The model can give a good prediction regardless test parameters.

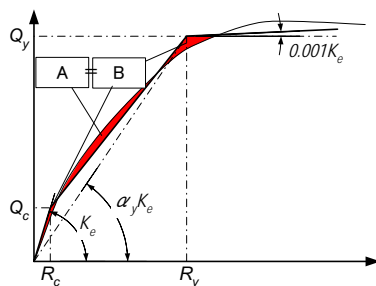


Figure 11 Skeleton curve

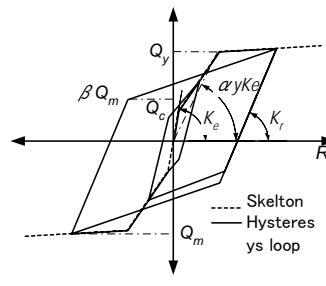


Figure 12 Hysteretic model

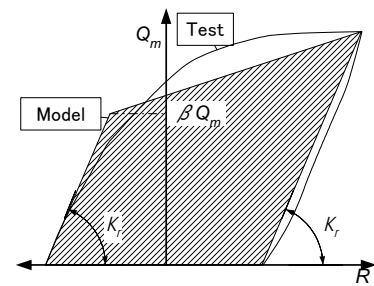


Figure 13 Definition of  $K_r$  and  $\beta$

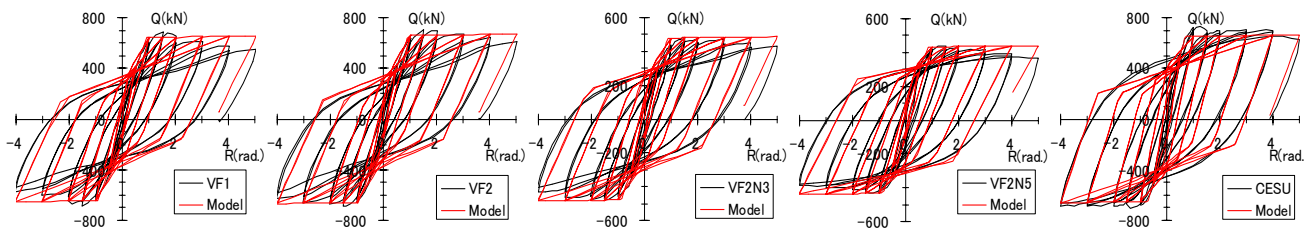


Figure 14 The comparative results of shear force–story drift angle relationship

## 5. CONCLUSIONS

In order to investigate the structural performance of CES structural systems, seven CES column specimens and six CES beam-column joint specimens were tested under lateral load reversals. From the tests, the following conclusions were obtained.

1. CES columns and joints had excellent seismic behavior without severe damage, even at large story drift angle,  $R$  of 0.04 rad. Using FRC for CES columns and beam-column joints, the ductility is improved and the damage of cover concrete is reduced.
2. The AIJ design formulas for SRC structures (AIJ 2001) can be applied for evaluating the ultimate flexural strengths of CES columns. The ultimate panel shear strengths for CES beam-column joints calculated by the AIJ design formulas tend to be smaller than the experimental values and thus are capable of safeguarding the design criteria.
3. A hysteretic model for the nonlinear behavior of CES columns was proposed. This model can accurately predict the hysteretic behavior of CES columns.

## REFERENCES

- Architectural Institute of Japan (AIJ). (1999). Standard for Structural Calculation of Reinforced Concrete Structures -Based on Allowable Stress Concept-  
Architectural Institute of Japan (AIJ). (2001). Standard for Structural Calculation of Steel Reinforced Concrete Structures -Based on Allowable Stress Concept and Horizontal Load-Carrying Capacity-